Agricultural and Forest Meteorology 249 (2018) 420–433

Contents lists available at ScienceDirect

Agricultural and Forest Meteorology

journal homepage: www.elsevier.com/locate/agrformet

Using a Bayesian framework to account for advection in seven years of snowpack CO_2 fluxes in a mortality-impacted subalpine forest

E.M. Berryman[a,*], J.M. Frank[b], W.J. Massman[b], M.G. Ryan[b,c]

[a] U.S. Geological Survey, Geosciences and Environmental Change Science Center, Denver, CO, United States
[b] USDA Forest Service, Rocky Mountain Research Station, 240 West Prospect, Fort Collins, CO 80526, United States
[c] Colorado State University, Natural Resource Ecology Laboratory, Fort Collins, CO 80524, United States

ARTICLE INFO

Keywords:
Soil respiration
Winter

ABSTRACT

In subalpine forests where snowpacks can persist for 50% of the year or longer, wintertime subnivean soil respiration constitutes a significant, but poorly understood, portion of the carbon (C) cycle. The temporal and seasonal dynamics of this flux are difficult to measure compared to snow-free respiration. This makes it challenging to fully address key knowledge gaps in high-elevation forests, including effects of tree mortality on ecosystem C fluxes. Our paper attempts to overcome these challenges by developing a new method for estimating wintertime CO_2 flux from soil underneath winter snowpack based on CO_2 profiles in the snow and using this to examine potential effects of a tree mortality event on wintertime respiration. The chief problem for estimates based on snow CO_2 measurements is that during strong winds, vertical CO_2 profiles can depart significantly from linearity, resulting in CO_2 fluxes that are not steady-state diffusive fluxes. Consequently, these fluxes include an advective component induced by wind and atmospheric pressure, resulting in above-snowpack fluxes that may be temporally decoupled from biological flux production in the soil. These advective fluxes lead to errors in estimates of the total amount of CO_2 produced from the soil surface during the winter, and may complicate the detection of significant seasonal and interannual trends in snowpack CO_2 fluxes. Our goal was twofold: first, to improve methods for estimating wintertime subnivean soil respiration; and second, to use this new method to examine potential effects of forest mortality on respiration. We develop a Bayesian-based model of CO_2 snowpack profiles and accounts for CO_2 storage flux within the snowpack to calculate diffusive and advective fluxes from both the bottom and the top of the snowpack. We apply this model to hourly snowpack CO_2 profile data collected over 7 years at an AmeriFlux eddy covariance (EC) site in a Wyoming subalpine forest that had recently experienced a mass tree mortality event. Hourly advective fluxes from the snowpack surface are less variable over time than hourly EC fluxes. Nonetheless, on a daily time scale, the two methods agree well with each other. We found that soil biological CO_2 production entering the bottom of snowpack peaked 3 years after the onset of the bark beetle outbreak and 1-year after dead trees dropped their needles, presenting the first evidence of a short-term increase in respiration following bark beetle mortality. Our findings emphasize the importance of accounting for the role of wind-driven advection in wintertime respiration and suggest that tree mortality may nearly double wintertime respiration in the first few years.

1. Introduction

Soil respiration, from plant roots and soil heterotrophs, is an indispensable measurement for terrestrial carbon (C) cycle research, but characterizing its variability across time and space is often a challenge (Ryan and Law, 2005; Phillips et al., 2016). Automated measurement techniques have allowed higher-resolution temporal measurements of soil respiration, advancing our understanding of diel, seasonal and interannual controls over this significant portion of the annual C budget (Carbone and Vargas, 2008; Vargas and Allen, 2008; van Asperen et al., 2017). However, in non-tropical areas, most of these advancements deal only with respiration during the growing season, leaving much to be understood about respiration during the winter. Wintertime respiration is especially important in seasonally snow-covered ecosystems where the insulative properties of snow keep soil temperature at or above freezing, maintaining biological activity (McDowell et al., 2000; McGuire et al., 2000; Brooks et al., 2004; Tucker et al., 2016). In fact, wintertime snowpack respiration may show some seasonality (Hubbard et al., 2005), which should be taken into account in sampling designs if the goal is to close annual C budgets. Improving our ability to capture

* Corresponding author. Current affiliation: US Forest Service Forest Health Assessment and Applied Sciences Team, Fort Collins, CO 80526, United States.
E-mail address: erin.berryman@cn-bus.com (E.M. Berryman).

https://doi.org/10.1016/j.agrformet.2017.11.004
Received 28 April 2017; Received in revised form 20 September 2017; Accepted 5 November 2017
Available online 10 November 2017
0168-1923/ Published by Elsevier B.V.

spatial and temporal variability in wintertime respiration is necessary to understand interannual dynamics of the C cycle in snow-dominated forests. Eddy covariance captures high (e.g., half-hourly) temporal variability in C fluxes, and its large footprint makes it a useful tool for aggregating spatial variability.

However, it is challenging to glean detailed information about wintertime soil respiration from EC. The method tends to have signal-to-noise issues with low CO_2 fluxes typical of wintertime (Webb et al., 2016). Also, EC fluxes at half-hourly timescales may not represent contemporaneous CO_2 production in the soil due to temporal dynamics of transport processes through snowpack, including advection (Euskirchen et al., 2012). Consequently, there is a need for an independent method to measure wintertime soil respiration underneath snowpack at a high temporal resolution similar to that of EC.

Automated measurements of snowpack CO_2 concentrations can be made at fine time scales (Seok et al., 2009), and these data can help address a major methodological challenge with measuring soil respiration that exits through the snowpack. Typically, wintertime soil respiration is calculated by applying Fick's first law of diffusion to a vertical CO_2 gradient measured in the snowpack (Sommerfeld et al., 1993; Hubbard et al., 2005), assuming steady-state conditions wherein flux emanating from the snowpack surface is equivalent to respiration from the soil into the snowpack. Under conditions where snowpack CO_2 concentrations are largely diffusion dominated, this method estimates soil respiration with high confidence. However, wind generates advective fluxes in which CO_2 is pumped from the surface layer of snow, generating non-linear CO_2 profiles that result in erroneous fluxes when only Fick's first law is used for calculation (Massman et al., 1995; Takagi et al., 2005; Bowling and Massman, 2011). Thus, we need some way to infer soil respiration into the bottom of the snowpack when advective fluxes from the snowpack surface create nonlinearity in snowpack CO_2 profiles. Measuring vertical snowpack CO_2 profiles at frequent (e.g., hourly) timescales can provide enough information to calculate (1) storage, advective and diffusive fluxes, (2) flux from the soil into the snowpack for ecological interpretation, and (3) flux from the top of the snowpack to the atmosphere for comparison to eddy covariance.

Despite its low magnitude, winter respiration may be an indicator of changing C cycle dynamics in forests that have experienced mass tree mortality events, but no results have been presented to date. Studies have found either no significant effect of bark beetle mortality on growing season soil respiration or only a modest, short-term change (Morehouse et al., 2008; Moore et al., 2013; Speckman et al., 2015; Borkhuu et al., 2015). Detecting change in growing season soil respiration is complicated by its sensitivity to short-term changes in soil temperature and moisture (Davidson et al., 1998) that may obscure mortality effects. However, microclimate forcings on respiration are lessened during the winter, when snowpack insulates the soil surface and maintains soil temperature slightly above freezing and holds soil moisture at a more constant level (Contosta et al., 2016). Thus, mortality impacts on respiration may be easier to detect in under-snowpack respiration compared to growing season soil respiration. We hypothesize that tree mortality effects on substrate availability for respiration will result in a noticeable increase in wintertime soil respiration underneath snowpack in the first few years following tree mortality from fine root mortality and needlefall.

One key challenge with ecological measurements that are made with high temporal frequency but low spatial replication is assigning measures of uncertainty. Calculation of soil respiration from vertical CO_2 profiles requires information about variables that influence the rate at which CO_2 moves through the snowpack. The precise values of these variables (e.g., snowpack temperature, porosity, and density) at the locations of CO_2 measurements are usually unknown; rather, they are estimated from nearby snow pits. These sources of uncertainty, even when not precisely known, can be taken into account in a Bayesian analytical framework. Having a reliable measure of uncertainty around these fluxes will allow a comparison between our snowpack CO_2 profile method and accompanying EC tower, as well as allowing the quantification of significance in observed variation of fluxes over time.

In this study, we calculate total CO_2 flux from the snowpack surface at hourly timescales to compare with contemporaneous half-hourly EC measurements. In addition, we examine factors related to overall flux uncertainty and the contribution of advective versus diffusive processes to total flux from the snowpack. Lastly, we hypothesize that the biological flux of CO_2 from soil into the bottom of the snowpack would increase as a result of the tree mortality event. To achieve this, we develop a Bayesian-based method to estimate both advective and diffusive components of CO_2 fluxes from both the bottom of the snowpack (interpreted as biological soil respiration) and from the top of the snowpack (comparable to eddy covariance measurements) and apply it over a 7-year time period at an AmeriFlux site located within a subalpine forest in the Rocky Mountains of southern Wyoming, USA, that had recently experienced tree mortality.

2. Methods

2.1. Study site and data collection

Research was conducted at the Glacier Lakes Ecosystem Experiments Site (GLEES) in southeastern Wyoming which is part of the AmeriFlux network of eddy covariance sites (US-GLE, ameriflux.lbl.gov). GLEES is a mature subalpine forest at 3190 m elevation and receives 1250 mm of average annual precipitation, about 80% as snow. Snowpack persists an average of 8 months per year; development typically begins in October and persists until June or July. Forest species composition consists of old growth Engelmann spruce (*Picea engelmanii* Parry ex Engelm.) with subalpine fir (*Abies lasiocarpa* (Hook.) Nutt.). A spruce bark beetle outbreak that peaked in 2008 caused 80–90% overstory spruce mortality; most trees died by 2010 and dead needles soon fell from the canopy (Frank et al., 2014).

In 2009, four 2-m tall mini-towers (Replicates 1 through 4) were erected within 0.25 ha of the eddy covariance tower for the purpose of measuring hourly vertical snowpack CO_2 profiles. Each tower consisted of 11 horizontal gas collector disks (Sommerfeld et al., 1991) with 0.2 m vertical spacing from the soil surface up to the top. Each disk was connected to a solenoid manifold which reduced the inlets through a single tube (Dekabon, 6.35 mm O.D., Synflex, Aurora, OH) that ran along the soil surface from the mini-towers to the AmeriFlux shelter at distances between 20 m and 40 m. Inside the shelter, snowpack air was pulled through a sampling system controlled by a micrologger (CR23X, Campbell Scientific, Logan, UT) and featuring a CO_2 analyzer (LI-800 until January 2015 then LI-820 afterward, LiCor Inc., Lincoln, NE). The sampling system pulled air through a magnesium perchlorate desiccant, monitored the volume of air pulled from each inlet, cut off the flow after air from each gas collector disk had filled the CO_2 analyzer, allowed the analyzer to equilibrate for 4 s, then measured the sample at 1 Hz for 20 s; internal averaging was turned off in the CO_2 analyzer. The system cycled through every inlet once an hour. Ancillary micrometeorological data for turbulence (u_*, ms^{-1}), and CO_2 flux ($\mu mol\ m^{-2}s^{-1}$) were taken from the co-located US-GLE AmeriFlux scaffold (Frank et al., 2014). Data quality was achieved through periodic calibrations of the CO_2 analyzer and the mass flow controller and omitting measurements from frozen inlets, frozen tubes, or meltwater contamination in the CO_2 analyzer, based on physical inspection and evaluation of summary statistics.

For calculation of fluxes from snowpack CO_2 concentrations, information about physical snowpack properties (density (ρ_{snow}), height (h), and temperature (T)) is required at the same temporal resolution as the hourly CO_2 measurements. Consequently, we estimate these at hourly timescales using a model that was driven by daily precipitation observations (P (m)) and constrained by field measurements of snowpack properties. The snow accumulation model was constructed by

simultaneously fitting two data sets: (1) the long term record of average daily snow heights observed at the US-GBT AmeriFlux site dating back to 2001, and (2) periodic snow pit density profiles measured around the US-GLE AmeriFlux scaffold on 10 occasions beginning in 2011. Snowpit density was obtained using a 1 L cutter (Snowmetrics, Fort Collins, CO, USA) to sample every 10 cm of depth and weighing the sampled snow to obtain its density. Because h was measured weekly at the replicates but continuously at only one nearby location, hourly h at the replicates was estimated using interpolation. T was measured at only a subset of depths and during just a few years, so instead it was estimated hourly by solving the heat equation for the snowpack described by the snow accumulation model and driven by atmospheric measurements. Further details of the snow accumulation model are found in Appendix A.

We took a conservative approach when applying this model to time periods outside the range of conditions represented by the snow pit samples; because our calculation of snowpack fluxes are sensitive to snowpack density, we did not calculate fluxes during snowpack collapse and ablation in late winter and early spring (as determined by comparing modeled snowpack height, $\hat{h}$, to the actual measurement h; see Appendix A). In addition, because shallow snowpack depth may affect respiration (Webb et al., 2016; Tucker et al., 2016), fluxes were calculated only from profiles that had CO_2 readings at four or more depths at each Replicate and time step which equated to at least a 0.8 m deep snowpack. Finally, data were often unavailable at the beginning of the winter due to repairs and frozen meltwater in the lines. As a result, fluxes were only calculated for the following time periods each year: December 15, 2009 – April 7, 2010; December 14, 2010 – May 4, 2011; February 2, 2012 – March 4, 2012; January 11, 2013 – April 17, 2013; January 1, 2014 – April 14, 2014; February 11, 2015 – March 3, 2015; and February 1, 2016 – March 31, 2016. After this data-filtering process, we were left with a total of 38,327 hourly profiles distributed across four spatial replicates from which to calculate respiration fluxes. We lacked usable data from Replicate 4 for 2010, 2014 and 2015.

Our analysis occurs in two phases: (1) deducing vertical advective and diffusive fluxes from vertical profiles of CO_2 (Section 3.2), and (2) analyzing snowpack fluxes for effects of year, Replicate, and turbulence (Section 3.3). For both phases, we use a hierarchical Bayesian framework that allows for complex models while accounting for random, systematic, and correlated uncertainty (Gelman et al., 2014). For phase 1), this statistical approach allows us to quantify the uncertainties in the diffusive, advective, and storage CO_2 flux terms. In phase 2), we use the Bayesian cut function (Plummer, 2015) to propagate these uncertainties.

2.2. Bayesian estimate of fluxes from CO_2 profile data

We use a 1-dimensional model [vertical dimension = z (m)] to estimate four CO_2 fluxes: the diffusive flux emanating from the top of the snowpack [$J_{diff}(1)$ (μmol-CO_2 $m^{-2}s^{-1}$)], the diffusive flux entering the bottom of the snowpack from the soil [$J_{diff}(0)$ (μmol-CO_2 $m^{-2}s^{-1}$)], and each of their respective advective counterparts, $J_{adv}(1)$ (μmol-CO_2 $m^{-2}s^{-1}$) and $J_{adv}(0)$ (μmol-CO_2 $m^{-2}s^{-1}$); where the top of the snowpack is denoted by $z/h = 1$, h (m) is the snowpack height, and the bottom of the snowpack (or the snowpack/soil interface) is denoted by $z/h = 0$. The model is also used to calculate the "storage flux" [S_{0h} (μmol-CO_2 $m^{-2}s^{-1}$)], analagous to the storage flux concept in eddy covariance calculations.

The model is developed in three steps, with details outlined in Appendix B. First, each hourly snowpack CO_2 profile is fit using the following analytical expression of a three-parameter error function (Eq. (1)).

$$\chi_c(z/h) = \chi_c(0) - \chi_B\left[\frac{\mathrm{erf}(\alpha z/h)}{\mathrm{erf}(\alpha)}\right] \equiv \chi_c(1) + \chi_B\left[1 - \frac{\mathrm{erf}(\alpha z/h)}{\mathrm{erf}(\alpha)}\right] \quad (1)$$

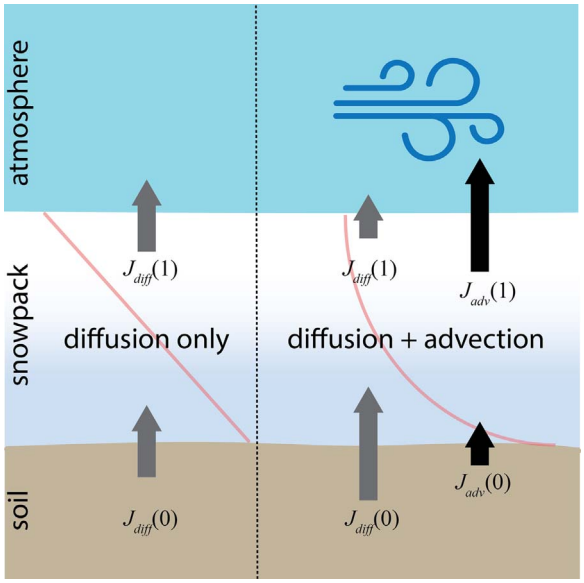

Fig. 1. Conceptual diagram of CO_2 fluxes through the snowpack (arrows) as related to CO_2 profile shape (light red lines) and presence of strong winds. The left side of the figure represents a steady-state scenario in which diffusion is the only driver of CO_2 movement from the soil and snowpack to the atmosphere and $J_{diff}(0) = J_{diff}(1)$. The right side of the figure represents a scenario with strong winds and a non-linear CO_2 profile. In this case, advection dominates the flux from the top of the snowpack to the atmosphere and steady-state assumptions result in erroneous calculations of soil to snowpack and snowpack to atmosphere CO_2 flux. (For interpretation of the references to color in this figure legend, the reader is referred to the web version of the article.)

where $\chi_c(z/h)$ (μmol-CO_2 (mol of dry air)$^{-1}$) is the snowpack CO_2 mixing ratio profile and $\chi_c(0)$ (μmol-CO_2 (mol of dry air)$^{-1}$), $\chi_c(1)$ (μmol-CO_2 (mol of dry air)$^{-1}$), χ_B (μmol-CO_2 (mol of dry air)$^{-1}$), and α (*dimensionless*) are model-fitting parameters determined for each of the hourly observed snowpack CO_2 profiles and erf is the error function. Only $\chi_c(0)$ or $\chi_c(1)$ need to be fitted, not both. This model form was chosen because of the physical interpretation of its parameters. $\chi_c(1)$ and $\chi_c(0)$ are the CO_2 mixing ratios at the top of the snowpack and at the snowpack/soil interface, respectively. χ_B is the difference between the two, i.e., $\chi_B \equiv \chi_c(0) - - \chi_c(1) > 0$. χ_B is relatable to the bulk snowpack CO_2 gradient $= -\chi_B/h$. Finally, α is the curvature parameter or a measure of how much the profile departs from linearity, as exampled in Figs. 2 and 3, and $\alpha \geq 0$. The mathematical expression of this property of α is $\lim_{\alpha\to 0} \mathrm{erf}(\alpha z/h)/\mathrm{erf}(\alpha) = z/h$ and, therefore, the profile $\chi_c(z/h)$ becomes a linear function of depth, $\chi_c(z/h) = \chi_c(0) - \chi_B z/h$, when $\alpha \equiv 0$. A linear profile indicates that CO_2 transport through the snowpack is by steady-state diffusion alone. Under this condition, $S_{0h} \equiv 0$, $J_{diff}(1) \equiv J_{diff}(0) \neq 0$, and $J_{adv}(1) \equiv J_{adv}(0) \equiv 0$ (Fig. 1). Thus, we can interpret α as a measure of the strength of the advective forcing. Finally, we should note that (1) the snowpack height $h = h(t)$ is assumed to be a function of time, t (s), throughout the season; but, as discussed in Appendix A, it is modeled externally and independently of the CO_2 profile model; and (2) the three fitting parameters should also be considered functions of time because they can vary from one CO_2 profile to another. This time dependency of these four model parameters is critical when estimating S_{0h}.

We use Eq. (1) to estimate the vertical CO_2 gradient $\frac{\partial \chi_c}{\partial z}$ (first derivative of the analytical profile), which is then combined with the modeled snowpack properties to estimate the diffusive fluxes, $J_{diff}(1)$ and $J_{diff}(0)$. The diffusive flux calculation takes the general form of

$$J_{\mathrm{diff}} = -\tau\eta\overline{\rho_d}D_{c0}\left(\frac{T_K}{T_{0K}}\right)^{0.81}\frac{\partial \chi_c}{\partial z} \quad (2)$$

where

(A) $\tau(z/h) = \tau = \overline{\tau} = 0.78$ (*dimensionless*) is the snowpack tortuosity

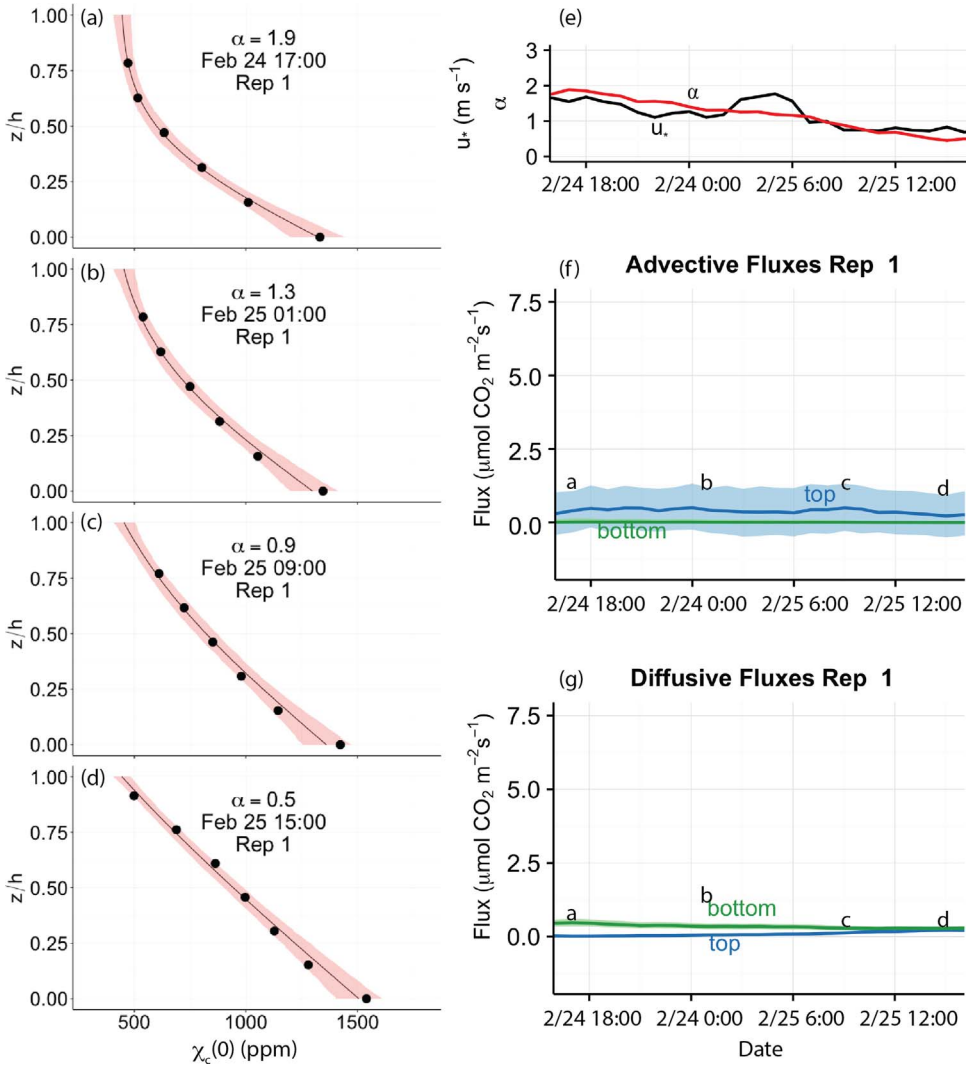

Fig. 2. Snowpack CO_2 profiles (a–d), corresponding u_* (e; black line) and α (e; red line), and calculated snowpack CO_2 fluxes (advective and diffusive, from the top and the bottom of the snowpack; f–g) over the course of 22 h in February 2010 at Replicate 1. For profiles, points are observations, and the line (median) and the bands (95% HDI) indicate the modeled values. The value of α for the fitted CO_2 profile is shown in each panel. z/h = height of measurement relative to total height of snowpack; $\chi_c(0)$ = partial pressure of CO_2. (For interpretation of the references to color in this figure legend, the reader is referred to the web version of the article.)

profile and is assumed uniform through out the snowpack;

(B) $\eta(z/h) = 1 - \rho_{snow}(z, t)/\rho_{ice}(T(z)) = 1 - \overline{\rho}_{snow}(t)/\rho_{ice}$ (*dimensionless*) is the porosity profile of the snowpack; where ρ_{ice} = 9.17 [kg m^{-3}] is the density of ice, $\rho_{snow}(z, t)$ (kg m^{-3}) is the bulk density profile of the snowpack (supplied externally by the snowpack model);

(C) $\overline{\rho_d}$ = 44.613 (mol m^{-3}) is the density of dry air at STP; $D_{c0} = 0.1381 \times 10^{-4}$ (m^{2}s^{-1}) is the diffusivity of CO_2 in dry air at STP; and $T_K(z/h)$ (K) is the snowpack temperature profile (modeled as part of the snowpack model discussed in Appendix A) and T_{0K} = 273.15 K.

Second, the storage flux (S_{0h}) (related to the time derivative of snowpack CO_2 mixing ratio) is computed by integrating the analytical profile over the depth of the snowpack and then used with finite difference techniques to determine S_{0h}.

$$S_{0h} = \int_0^1 \frac{\partial \rho_c}{\partial t} dz \equiv \overline{\rho_{da}} \int_0^h \frac{\partial \chi_c}{\partial t} dz \quad (3)$$

where $\rho_c = \rho_c(z)$ (μmol m^{-3}) is the snowpack profile of CO_2 molar concentration and $\overline{\rho_{da}}$ is the ambient dry air density ($\overline{\rho_d}$ corrected for ambient pressure and temperature). At GLEES $\overline{\rho_{da}} \approx 32$ mol m^{-3}. Details of finite differencing are presented in Appendix B.

Third, we combine the mass conservation law for snowpack CO_2 with $J_{diff}(1)$, $J_{diff}(0)$, S_{0h} and a simple 1-d model relating $J_{adv}(1)$ and $J_{adv}(0)$ (using a parameter (β) to partition between the two) to estimate each of these two advective fluxes separately.

$$S_{0h} = J_{diff}(0) - J_{diff}(1) + J_{adv}(0) - J_{adv}(1) \quad (4)$$

We assume that there are no sources or sinks of CO_2 within the snowpack; i.e., that no CO_2 moving through the snowpack is adsorbed/desorbed by the snow ice surfaces or that it is produced or destroyed chemically by any other compounds on the snow ice surfaces or within the snowpack atmosphere. While a possible scenario, especially for CO_2 uptake into liquid water in the snowpack, it is one for which we have little data to inform.

The final step is parameterizing the advective fluxes so that Eq. (4) can be solved algebraically for the two advective fluxes. This requires a relationship between $J_{adv}(1)$ and $J_{adv}(0)$ that is physically reasonable, numerically robust, and produces a mathematically tractable problem.

$$J_{adv}(0) = \beta\alpha J_{adv}(1) \quad (5)$$

We assume that β = 0.02, a constant with a range of uncertainty between 0.002 and 0.2. This value for β is heuristic and arbitrary; β selection and rationale are discussed in more detail in Appendix B.

Combining Eqs. (4) and (5) yields:

$$S_{0h} = J_{diff}(0) - J_{diff}(1) - J_{adv}(1)(1 + \beta\alpha) \quad (6)$$

Now all five flux terms of Eq. (4) can be estimated for every hour of CO_2 profile measurements. This allows (1) estimates of the total flux exiting the top of the snowpack, $J_{diff}(1) + J_{adv}(1)$, to be compared with simultaneously measured eddy covariance fluxes; and (2) the interpretation of the flux entering the bottom of the snowpack, $J_{diff}(0)$

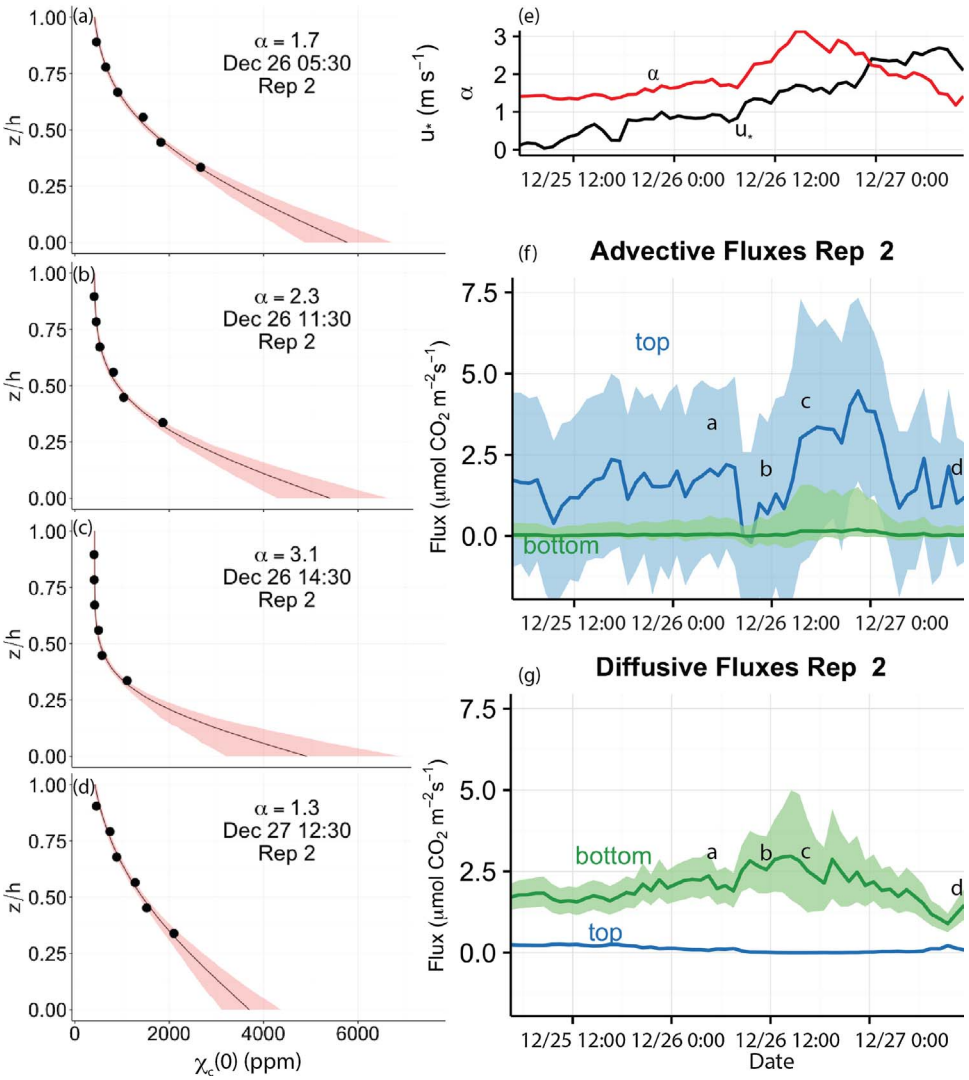

Fig. 3. Snowpack CO_2 profiles (a–d), corresponding u_* (e; black line) and α (e; red line), and calculated snowpack CO_2 fluxes (advective and diffusive, from the top and the bottom of the snowpack; f and g) over the course of 2.5 days in December 2010 at Replicate 2. For profiles, points are observations, and the line (median) and the bands (95% HDI) indicate the modeled values. The value of α for the fitted CO_2 profile is shown in each panel. In contrast to Fig. 2, turbulence increased over this time period and Replicate 2 has no measured value for $\chi_c(0)$. z/h = height of measurement relative to total height of snowpack; $\chi_c(0)$ = partial pressure of CO_2. (For interpretation of the references to color in this figure legend, the reader is referred to the web version of the article.)

$+ J_{adv}(0)$, as the wintertime soil respiration flux.

We used a Bayesian approach to fit each unique vertical CO_2 profile to Eq. (1) as follows. Each snowpack CO_2 measurement was predicted from z using a normal distribution with a mean defined by Eq. (1) and a heteroscedastic standard deviation defined as the product of that mean multiplied by ϵ. A unique set of model parameters were determined for each vertical profile and all were given prior probabilities defined as gamma distributions with an expected value $\pm \sqrt{\text{variance}}$: α (2 ± 1.5), χ_B (2000 ± 100 ppm), and $\chi_c(1)$ (450 ± 25 ppm). All profiles shared the same value for ϵ which was also given a gamma prior distribution $\left(\frac{1}{\sqrt{10}} \pm \frac{1}{\sqrt{10}}\right)$. The posterior distributions for α, χ_B, $\chi_c(1)$, and ϵ were determined using JAGS (version 4.2.0, Plummer, 2003) using an approximation for the error function (Schöpf and Supancic, 2014) within R (version 3.3.2) (Core Team, 2016) with packages *rjags* (Plummer, 2017) and CODA (Plummer et al., 2006). Posterior distributions were constructed using Markov Chain Monte Carlo (MCMC) sampling (Kruschke, 2014) by running three chains, initializing for 100 steps, burn-in for 5000 steps, sampling for 10,000 steps, and thinning the final chain to retain 1 out of every 10 samples. Because of the sheer number of unique profiles, it was impractical to inspect each MCMC chain for convergence via trace plots or other visual diagnostics. While this was done for a random subset of parameters during beta testing of the MCMC settings, convergence was investigated by inspecting the summary statistics (mean, standard deviation, quantiles) of all posterior distributions with respect to time and Replicate.

Then, using the posterior distributions associated with each profile (α, χ_B, and $\chi_c(1)$), fluxes were calculated for each hour and Replicate according to Eqs. (2), (4), (5) and (6) in Appendix B. The parameter β was given a prior distribution with an expected value of 0.02 that spanned the range of 0.002–0.2. This was achieved by $\beta = 2 \times 10^{(2n-3)}$ where n is given a beta distribution with an expected value $\pm \sqrt{\text{variance}}$ of 0.5 ± 0.224. Unlike the other model parameters, there is no information in our model to constrain the value of β based on data. Instead, we sample β directly from this prior distribution in order to account for its contribution to our uncertainty in estimating advective fluxes.

2.3. Bayesian hypothesis testing of snowpack flux

We then performed hypothesis testing about the temporal variability in respiration from the bottom of the snowpack using a Bayesian analysis. We relate fluxes to year (y), Replicate (r), and coincident friction velocity from the Ameriflux eddy covariance tower (u_*). Soil temperature, while important for respiration during time periods where the temperature fluctuates more than 1 °C, varied little during this study due to thick and stable snowpack (see Section 3.1) and thus was not included in the model. The model predicts $J(0) = J_{diff}(0) + J_{adv}(0)$ for every year, Replicate, and time (i, hours) from a normal distribution with a mean defined in Eq. (7) and a standard deviation ε.

$$\hat{J}(0)_{y,r,i} = \theta_y x_y \times \theta_r x_r + \theta_{u_*} u_{*i} \quad (7)$$

The first term in Eq. (7) is the interaction between year and Replicate where x_y and x_r are nominal predictor variables (Kruschke, 2014) that categorically select the appropriate model parameters θ_y and θ_r for the year and Replicate of $J(0)$. The last term is u_* with the model parameter θ_{u_*}. A different θ_y is defined for each year, and all are given a prior gamma distributions. These distributions are hierarchical and share hyperparameters for their expected value (E) and variance (var); both of these are given prior gamma distributions with expected value $\pm \sqrt{\text{variance}}$ equal to 0.5 ± 0.5. This hierarchy forces a relationship between the year parameters. A different θ_r is defined for each Replicate with a prior normal distribution with mean ± standard deviation of 1 ± 0.5; θ_r acts as a random effect that proportionally adjusts the year effect. θ_{u_*} is given a prior normal distribution with mean ± standard deviation of 0 ± 0.1. The data prediction error ε was given a gamma prior distribution with expected value $\pm \sqrt{\text{variance}}$ equal to 1 ± 1.

In order to preserve the uncertainties associated with all fluxes while conducting hypothesis testing, we use the Bayesian cut function (Plummer, 2015). Conceptually, the cut function acts as a control valve that allows information to flow from the flux calculations to the hypothesis testing while preventing a flow of information in the reverse direction. This is relevant to our study as we do not desire the act of estimating θ_y, θ_r, and θ_{u_*} to influence the estimates of α, χ_B, and $\chi_c(1)$. The cut function is also useful in modularizing Bayesian analyses by creating a framework to combine summary statistics from previous analyses (Plummer, 2015). In our case, due to computational limitations it was impractical to estimate CO_2 fluxes from profiles while simultaneously conducting hypothesis testing. To implement the cut function using JAGS, we iteratively sampled from the CO_2 flux posteriors before conducting a full JAGS analysis of our hypotheses test; afterwards we combined the final values for θ_y, θ_r, and θ_{u_*} from each iteration into a single posterior chain (Plummer, 2011). We performed 3000 iterations of the cut function, sampling each step from the posterior α, χ_B, and $\chi_c(1)$ MCMC chains exactly once. Within each cut, we performed an MCMC analysis using JAGS with two chains, initialized for 10 steps, burned-in for 500 steps, sampled for 250 steps, and retaining only the final step. While these chains may appear short, the general principle of the cut function is to update the "cut" parameter infrequently while allowing all the other parameters to fully converge (Plummer, 2015). Here, for every one update of α, χ_B, and $\chi_c(1)$, the parameters θ_y, θ_r, and θ_{u_*} are allowed to converged over 760 steps. Statistical significance of the parameters was determined from their posterior 95% highest density intervals (HDI) by comparing against 0 for the null hypothesis or testing for overlaps with other parameters (Kruschke, 2013).

We tested the full model (Eq. (7)) against the following progressively simpler models:

$$\hat{J}(0)_{y,r,i} = \theta_y x_y \times \theta_r x_r \tag{8}$$

$$\hat{J}(0)_{y,r,i} = \theta_y x_y \tag{9}$$

$$\hat{J}(0)_{y,r,i} = F_0 \times \theta_r x_r + \theta_{u_*} u_{*i} \tag{10}$$

$$\hat{J}(0)_{y,r,i} = F_0 + \theta_{u_*} u_{*i} \tag{11}$$

$$\hat{J}(0)_{y,r,i} = F_0 \times \theta_r x_r \tag{12}$$

$$\hat{J}(0)_{y,r,i} = F_0 \tag{13}$$

where F_0 serves as a constant in place of the year effect.

To determine the best-fitting model, we used Deviance Information Criterion (DIC) (Spiegelhalter et al., 2002, 2014). An important consideration is that DIC can only be used to compare between models predicting the exact same data. Since our implementation of the cut function iteratively samples the CO_2 flux posteriors, only DIC values corresponding to identical sets of $J(0)$ can be compared. To accommodate this, we organized our DIC analysis as: (A) begin an iteration by sampling a set of $J(0)$ from the posterior distributions, (B) run a JAGS analysis for the full and simpler hypothesis models, (C) determine the minimum DIC value among these models, (D) rescale to ΔDIC by subtracting that minimum from all of the DIC values, (E) perform the rest of the iterations, and (F) for each model combine the ΔDIC values across all iterations into a distribution. By definition $DIC = p_D + \overline{D}$ where p_D is the effective number of parameters and $\overline{D}$ is the expectation of model fit (Spiegelhalter et al., 2002). Except for their contribution to ΔDIC, neither $\overline{D}$ nor DIC have any intrinsic meaning and thus are not reported, though we do report p_D. We choose the best model qualitatively using relative ΔDIC similar to the approach in Frank et al. (2013) who showed that large sample size can render traditional interpretations of ΔAIC unreliable. Instead, the best model is chosen through forward selection by including terms that result in large relative decreases in ΔDIC. The median and 95% HDI was used to determine the best fit (i.e., lowest ΔDIC) model. Parameters are described only for the best-fitting model and are denoted in the text as "median (2.5%, 97.5%)."

2.4. Comparison to other flux estimates

We compared our estimates to contemporaneous net ecosystem exchange (NEE) fluxes from the EC tower using Pearson correlation (R) at different timescales: hourly snowpack fluxes with hourly EC averages, and daily, weekly, and annual averages of both.

We also compared our flux estimates to those calculated from measurements made prior to our study at the same site. Past work at GLEES has captured higher spatial variability than ours (Berryman et al., 2016) and provides a good check for the representativeness of our estimates. Further, to help detect changes following bark beetle mortality, we assessed year-to-year dynamics of snowpack CO_2 fluxes prior to the time period studied here (2010–2016). Previously-published flux estimates from forested plots at GLEES were measured in 1991–1992 (Sommerfeld et al., 1993), 2002 (Musselman et al., 2005), and 2004–2005 (Berryman et al., 2016). Fluxes were also estimated from CO_2 concentrations collected from the bottom and top of the snowpack in 2006–2007 and 2009–2010 from the same forested plots and using the same methodology as Berryman et al. (2016). Similar data collected from forested areas at and near GLEES in 1998–1999 were also used to calculate fluxes for comparison to ours.

For calculations from these data, because we had no information about the shape of the CO_2 profile, we assumed a linear profile from the bottom of the snowpack to the top and calculated diffusive flux only by modifying Eq. (2) per the following:

$$J_{\text{diff}} = -\tau\eta\overline{\rho_d} D_{c0} \left(\frac{T_K}{T_{0K}}\right)^{0.81} \frac{\Delta\chi_c}{\Delta z} \tag{14}$$

where all parameters are as defined in Eq. (2), except:

(E) $\frac{\Delta\chi_c}{\Delta z} = \frac{\chi_c(0) - \chi_c(1)}{0 - h}$, where $\chi_c(0)$ is the reported CO_2 partial pressure at the bottom of the snowpack and $\chi_c(1)$ is the reported CO_2 partial pressure at the top of the snowpack, assumed to be the most recent ambient atmospheric measurement when not recorded for that specific point.

In other words, the same input data were used as for Eq. (2), except that we calculated fluxes by assuming a linear CO_2 profile and ignored the advective component. T_K was estimated as the mean of snow temperature at the bottom of the snowpack (assumed to be 0 °C on days when measurements did not exist) and air temperature in the hour nearest the time of CO_2 measurement (obtained from a weather station at GLEES). Snowpack density was not always measured on the same day as the CO_2 measurements; to standardize our approach, we assumed that $(\tau)(\eta)$ had a constant value of 0.55. Finally, we assessed the error inherent in assuming a linear profile by also calculating diffusive fluxes from the CO_2 profile data per Eq. (14) above. Error was calculated using

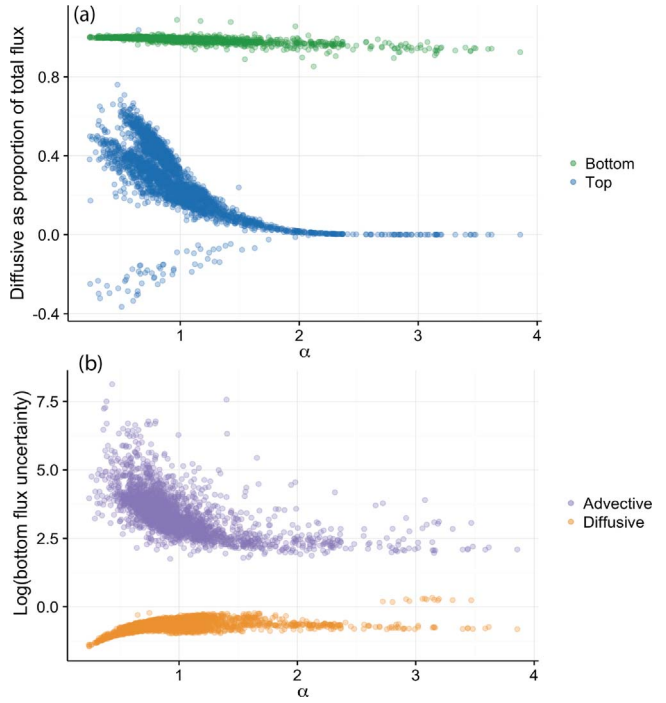

Fig. 4. For Replicate 1 in 2010, (a) the proportion of total flux (bottom and top) made up by the diffusive component plotted against α, and (b) log of the flux uncertainty (95% HDI range divided by the median) plotted against α. Negative values in Fig. 3(a) are a result of an artefact in the model which generates high uncertainty in advective fluxes which pushes the median of the posterior to a negative value large enough to cause the total flux from the snowpack to be negative.

root mean squared error (RMSE) between the hourly median predicted flux from a linear profile and the hourly median predicted flux using our nonlinear model.

3. Results

3.1. CO_2 Profile model

The shape of the CO_2 profile with depth in the snowpack varied over time, sometimes fluctuating between linear and concave shapes within the course of less than a day (i.e., Fig. 2a–d). The profile shape is reflected by α in the profile model (Eq. (1)), with high α corresponding to high concavity in the profile shape. Because concave profiles had low CO_2 gradients at the top of the snowpack and high CO_2 gradients at the bottom of the snowpack (Fig. 3), per Fick's first law of diffusion, these profiles had low diffusive fluxes at the top of the snowpack and high diffusive fluxes at the bottom of the snowpack. In these cases, advective flux from wind removal of CO_2 from the snowpack is a dominant process (Fig. 4). Concave CO_2 profiles were generally indicative of turbulent time periods, but high turbulence did not always lead to high advective flux from the top of the snowpack (e.g., Fig. 3e and f). There was a significant time-lagged correlation between α and u_* that was highest 1–4 h prior to profile measurements (Pearson correlation coefficient = 0.4).

Advective plus diffusive fluxes from the soil into the snowpack calculated using our model were on average 0.15 μmol CO_2 $m^{-2}s^{-1}$ greater than diffusive fluxes through the snowpack calculated assuming a linear profile. Root mean squared error between the two methods was 0.26 μmol CO_2 $m^{-2}s^{-1}$.

3.2. Flux uncertainty and accounting for advection

Soil respiration from the soil into the snowpack ($J_{diff}(0)$ and $J_{adv}(0)$) and snowpack CO_2 flux into the atmosphere ($J_{diff}(1)$ and $J_{adv}(1)$) calculated by our model typically ranged from 0 to 1 μmol CO_2 $m^{-2}s^{-1}$ but sometimes exhibited higher rates accompanied by large 95% HDI (Fig. 5). High uncertainty in the parameters of the CO_2 profile model begat high uncertainty in resulting fluxes; generally, flux uncertainty increased with increasing concavity (Fig. 4). However, the highest flux uncertainties expressed as a percentage of the median were attributed to missing CO_2 values from the bottom of the snowpack when CO_2 profiles were concave, i.e., an extrapolation issue (Fig. 3).

Even when advective flux from the top of the snowpack was high, the advective flux at the bottom remained small per Eq. (5), so diffusive flux dominated respiration at the bottom of the snowpack (Figs. 2 and 3). Advective fluxes out of the top of the snowpack were often slightly negative in magnitude but in most cases were overwhelmed by positive diffusive flux so that the net flux out of the snowpack was positive. However, in a few cases, the diffusive flux was not high enough and this resulted in a negative total flux out of the snowpack (Fig. 4a). In these cases, the 95% HDI of the advective flux overlapped with zero.

Hourly averaged EC fluxes were positively correlated with simultaneous advective plus diffusive CO_2 flux into the atmosphere ($R = 0.06$, $P < 0.001$). Pearson correlation coefficients increased for daily, weekly and annual flux averages ($R = 0.20$, $P < 0.001$; $R = 0.25$, $P < 0.001$; $R = 0.37$, $P < 0.05$).

3.3. Interannual trends in respiration

The range of calculated respiration fluxes from the bottom of the snowpack compared well to previous diffusive flux measurements at GLEES, though fluxes from our study exhibited more interannual variability than past measurements (Fig. 6). The model that explained most of the variance in soil respiration from the soil into the snowpack ($J_{diff}(0)$ and $J_{adv}(0)$) accounted for differences by year, Replicate and u_*; however, including u_* decreased DIC by a very small amount relative to the year and Replicate effect, and thus the most appropriate model was determined to only account for differences by year and Replicate (Fig. 8). Annually aggregated wintertime soil respiration is analogous to θ_y parameters from Table 1. The highest respiration was in 2011 (0.77 (0.55, 0.99) μmol CO_2 $m^{-2}s^{-1}$), one year following the needlefall of most dead trees, and 2013 had the lowest respiration (0.26 (0.18, 0.33) μmol CO_2 $m^{-2}s^{-1}$; Table 1).

4. Discussion

Using 38,237 hourly measurements of snowpack CO_2 profiles over the course of 7 years, we constructed a detailed time series of wintertime soil respiration, and CO_2 fluxes out of the snowpack, in a subalpine forest in southern Wyoming, USA following a bark beetle mortality event during which 75% to 85% of the tree canopy was lost (Frank et al., 2014). Our work builds upon a strong history of snowpack CO_2 research at this site (Sommerfeld et al., 1993, 1996; Massman et al., 1997; McDowell et al., 2000; Musselman et al., 2005). Despite methodological differences with past studies, our method yielded wintertime respiration values that were largely within the range of variability of past findings at the site (Fig. 6). However, our approach provides some key advantages over these previous efforts. Past estimates required manual measurements or collection of gas samples from the snowpack for later analysis, thus limiting the number of measurements that could be made and restricting the temporal resolution of measurements. Automated measurement increases the temporal resolution, allowing a detailed examination of temporal dynamics of wintertime soil respiration and CO_2 flux exiting the snowpack (Fig. 5). Further, past manual survey methods assumed that CO_2 flux out of the snowpack was diffusive only, so only air from the atmosphere and from the bottom of the snowpack were measured, providing no information about the linearity of the snowpack CO_2 profile. Our approach characterizes the non-linearity of these profiles at a high temporal resolution, quantifying advective and diffusive components, thus allowing accurate estimation of

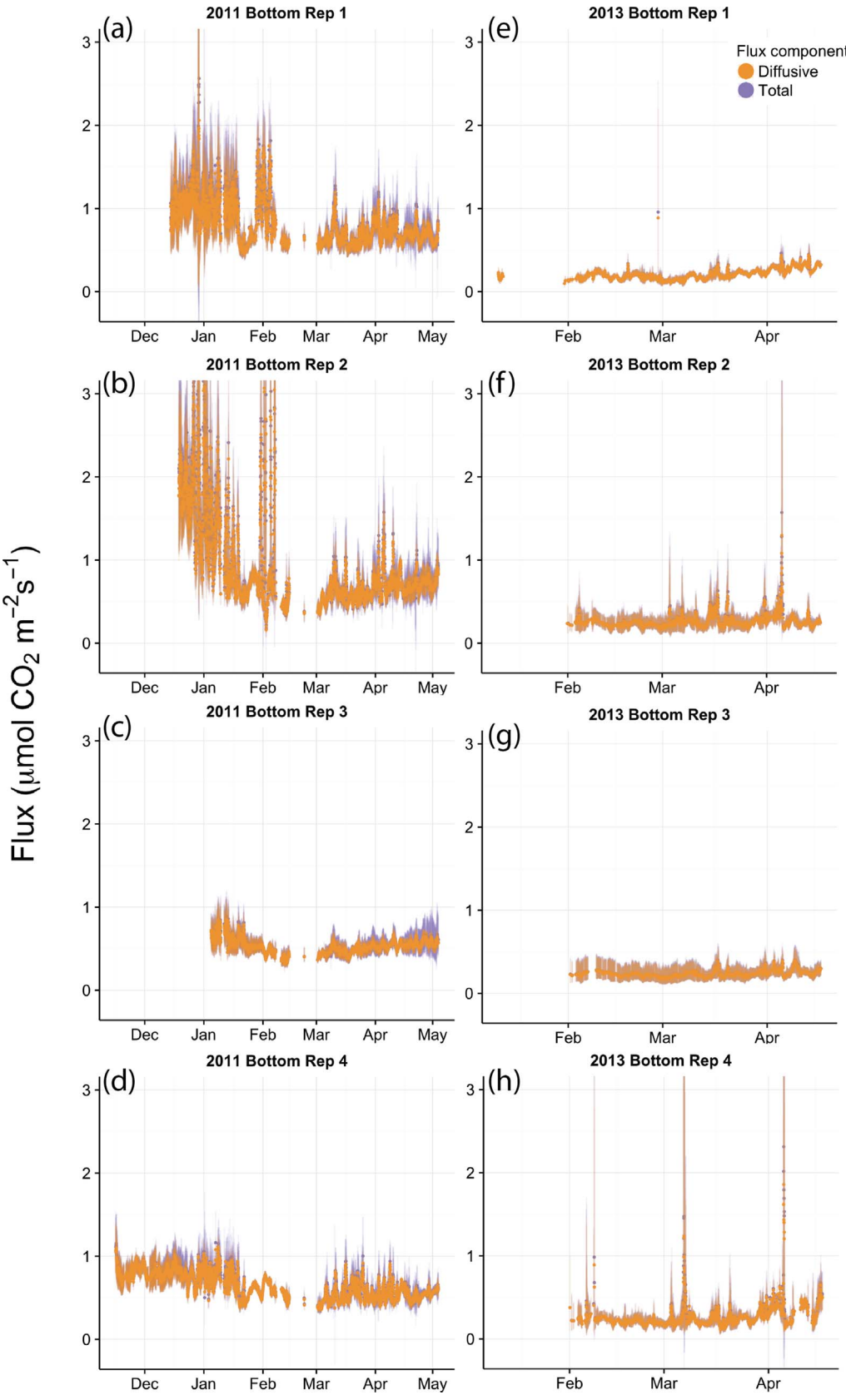

Fig. 5. Time series of total and diffusive (overlaid on total) CO_2 flux from the bottom of the snowpack and the 95% HDI (bands) for each active Replicate in 2011 (a–d) and 2013 (e–h).

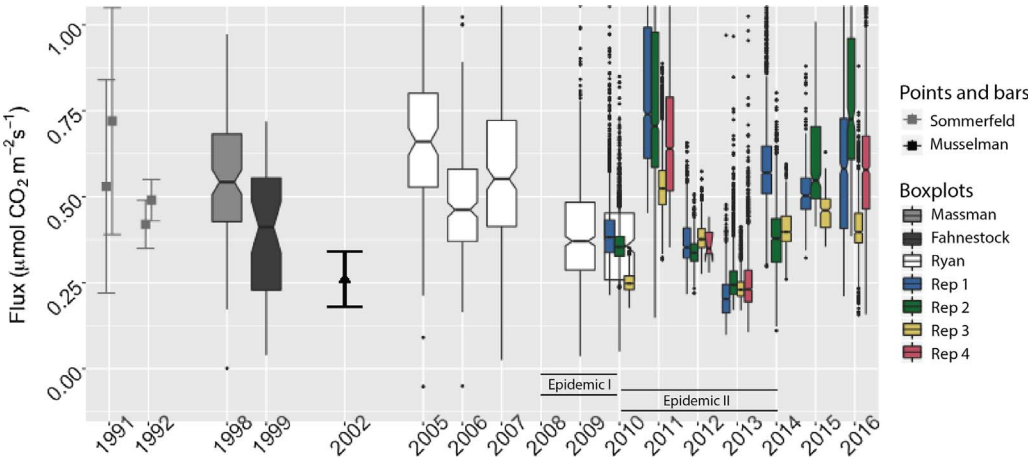

Fig. 6. Annual time series of diffusive fluxes previously measured at GLEES and minitower fluxes as presented in this paper. 1991–1992 values are mean ± 1 estimated standard deviation reported by Sommerfeld et al. (1993) using weekly measurements throughout each winter from two subalpine forested plots near present-day minitower locations. 2002 value is mean ± 1 standard deviation from four sampling dates reported by Musselman et al. (2005) in a forested site near present-day minitower locations. 1998–99 boxplots are measurements from forested areas near GLEES (two to four sampling dates per year and 17–30 locations per sampling date); 2005–06 fluxes are from Berryman et al. (2016) and 2007–10 fluxes are measurements from same plots (two sampling dates per year and 20 plots per sampling date). Fluxes from our study are separated out by Replicate and represent the median of the posterior calculated fluxes at each time step from the bottom of the snowpack (advective + diffusive). Notches in boxplots estimate 95% confidence intervals. Due to freezing in the inlet tubes, we lacked usable data from Replicate 4 for 2010, 2014 and 2015. Timing of the bark beetle outbreak is indicated by labels "Epidemic I" (trees began to die) and "Epidemic II" (trees dropped foliage) as determined by (Frank et al., 2014).

both CO_2 flux out of the snowpack and under-snowpack soil respiration.

4.1. Importance of advection and comparison to eddy covariance

The high temporal and vertical resolution of our CO_2 measurements made it possible to accurately calculate advective flux out of the top of the snowpack at a time scale comparable to that of the co-located eddy covariance (EC) tower. The two methods agreed with each other at daily, weekly, and annual time scales, but the correlations were weak and CO_2 flux out of the top of the snowpack varied substantially less over hourly and daily time periods than those from the EC tower (Fig. 7). Likely causes of high EC noise are the imperfect application of

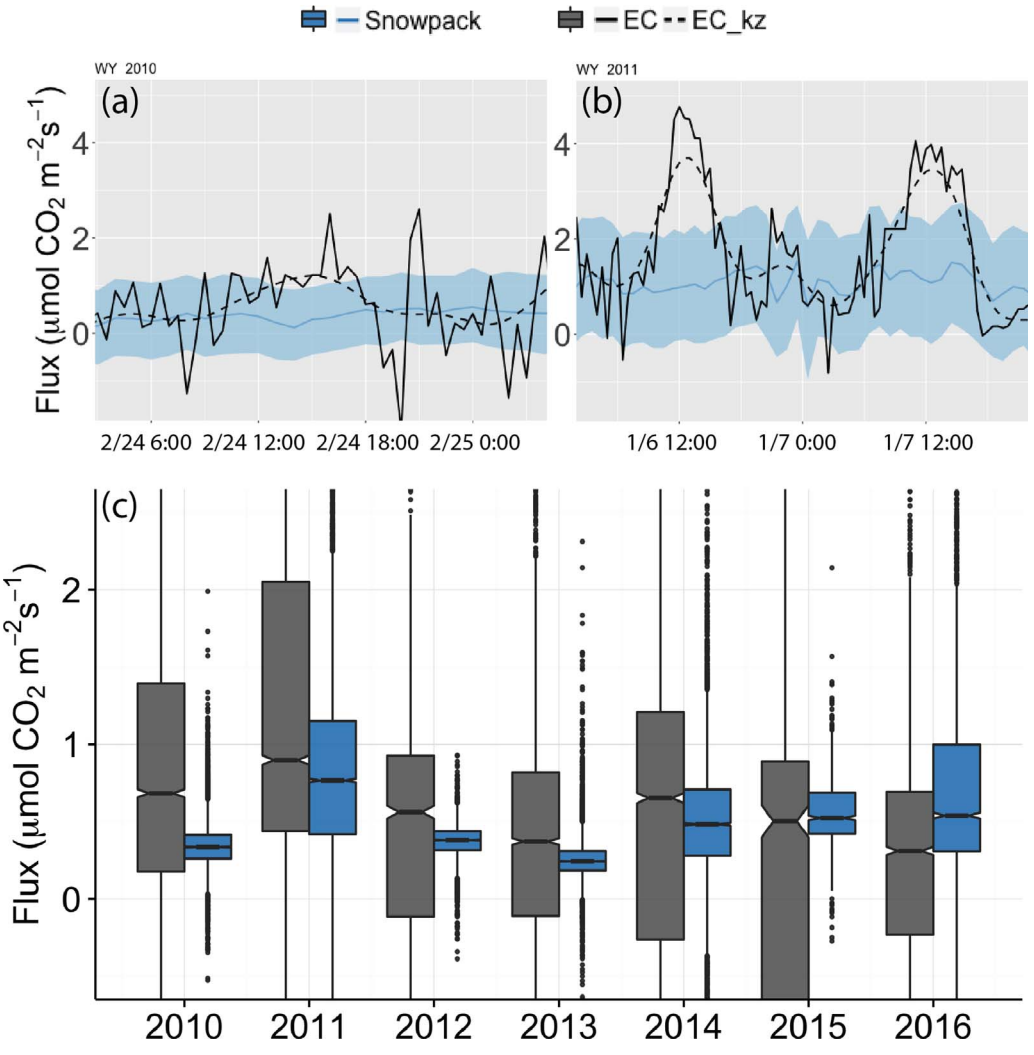

Fig. 7. Comparison of wintertime CO_2 fluxes from the top of the snowpack to net ecosystem fluxes measured by the accompanying eddy covariance (EC) tower. (a) and (b) Blue lines and bands represent time series of Replicate 1 in February 2010 and Replicate 2 in January 2011 (median ± 95% HDI); black solid lines are half-hourly NEE measurements from the EC tower and dashed lines are kz-smoothed EC measurements using a window of 3 h and $k = 3$ iterations. (c) Boxplots of each type of measurement by year in the study, showing the median and interquartile range of all the time steps that were measured. Snowpack data are medians of posterior calculated fluxes at each time step. (For interpretation of the references to color in this figure legend, the reader is referred to the web version of the article.)

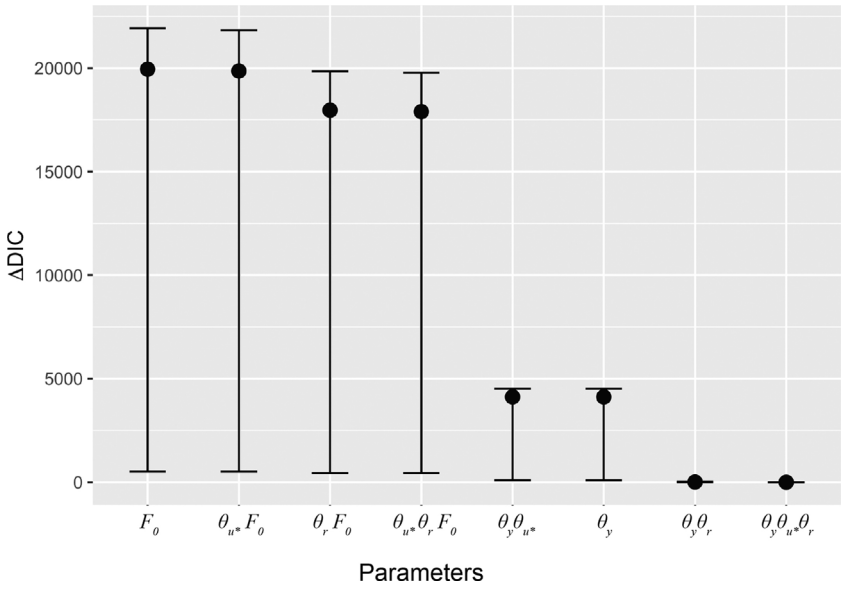

Fig. 8. Results of DIC analysis comparing the full model explaining temporal variability in total flux from the bottom of the snowpack to different reduced models. Values presented are the median (2.5%, 97.5%) of the difference in DIC between that model and the model with the lowest DIC for each MCMC step.

Table 1
Highest density intervals (HDI) for parameters from the best-fitting model according to Fig. 8. Year and replicate parameters in the same group have 95% HDI that do not overlap with each other.

Parameter	2.5%	Median	97.5%	Group
$\theta_{y,2010}$	0.25	0.34	0.44	ab
$\theta_{y,2011}$	0.55	0.77	0.99	cd
$\theta_{y,2012}$	0.26	0.36	0.47	ab
$\theta_{y,2013}$	0.18	0.26	0.33	a
$\theta_{y,2014}$	0.33	0.45	0.58	abc
$\theta_{y,2015}$	0.38	0.54	0.70	bcd
$\theta_{y,2016}$	0.47	0.64	0.84	cd
$\theta_{r,1}$	0.82	1.11	1.47	a
$\theta_{r,2}$	0.84	1.13	1.49	a
$\theta_{r,3}$	0.56	0.75	1.00	a
$\theta_{r,4}$	0.66	0.89	1.17	a
ϵ	0.22	0.25	0.83	

the analyzer self-heating correction for cold climates (Burba et al., 2008), variability of non-stationarity, and the additional contribution of respiration from trees above the snowpack detected by EC but not the snowpack minitowers. However, aboveground winter respiration is expected to be much lower than soil respiration due to exposure to temperatures that are well below freezing, and it would have been further reduced by live foliage moving from the canopy to the forest floor during the mortality event (Speckman et al., 2015). Although EC has the added benefit of being able to account for all of ecosystem respiration, to which soil respiration contributes, our snowpack CO_2 gradient method yielded more robust estimates of wintertime respiration than EC that may be more useful for detecting significant temporal shifts in respiration.

Highly dynamic CO_2 profiles and fluxes over time were linked to turbulent conditions as indicated by high u_* (Fig. 3), consistent with previous findings that wind-caused advection results in erratic CO_2 fluxes from the snowpack over short time periods (Takagi et al., 2005; Bowling and Massman, 2011). In most replicates and years, there was a correlation between α and u_* measured 1–4 h prior, but the correlation was not as strong as expected. A possible reason for this is illustrated in Fig. 3. Initially, as u_* and α rose during the first day, the advective flux from the top of the snowpack increased in response. However, with further increases in u_* approaching December 27th, advective flux from the top of the snowpack (and α) actually decreased. This response is consistent with the idea of wind-driven pumping of CO_2 from the snowpack which depletes the storage reservoir of CO_2. Further increases in turbulence cannot influence the storage flux as much because there is simply less CO_2 to pump out of the snowpack. This situation highlights the dynamic relationship among turbulence, snowpack CO_2 concentrations, and advective fluxes from the top of the snowpack and suggests that fluxes of CO_2 from the snowpack cannot be simply predicted from wind or turbulence measurements. Rather, high temporal resolution measurements of CO_2 are necessary to quantify the change in storage that can be a major contributor to advective CO_2 fluxes from the top of the snowpack.

Despite the weakness of the correlation between α and u_*, its lagged nature gives us more information about the system. High α following increases in u_* reduces the CO_2 gradient in the upper part of the profile which temporarily reduces diffusive flux from the top and creates a buildup of CO_2 at the bottom of the snowpack. Afterwards, "refilling" of the snowpack to a linear profile may take several hours, resulting in the lagged correlation between profile shape and turbulence. Another result of high u_* is high diffusive flux at the bottom of the snowpack relative to advective flux. Due to conservation of mass and relatively lower changes in snowpack storage CO_2 flux, high α indicates high advective flux out of the top of the snowpack. Consistent with this idea, α was indicative of the ratio of diffusive flux to advective flux, with higher values reflecting a dominance of advective vs diffusive flux out of the top of the snowpack (Fig. 4). Thus, the relative importance of advection for snowpack CO_2 fluxes can be surmised by inspecting the degree of linearity in the vertical snowpack CO_2 profile and the timescales over which the shape of the profile chages. Vertical inhomogeneities in ρ_{snow} can also result in nonlinear profiles (Mast et al., 1998). However, the shape of our CO_2 profiles changed over a matter of hours; ρ_{snow} cannot change that quickly, so we surmise that advection is the main cause of nonlinear CO_2 profiles in our study.

4.2. Flux uncertainty and detecting a mortality signal

One novel aspect of our approach is a Bayesian characterization of uncertainty in wintertime soil respiration. Such uncertainty was typically reasonable, provided (1) deep snowpack so that at least four depths had CO_2 measurements to inform our three-parameter model, and (2) reliable estimates of CO_2 near the bottom of the snowpack. When the bottom-most depths had usable measurements, even the most extreme windy conditions yielded reasonably low uncertainties (95% HDI were typically ± 25% of the median). However, CO_2 values from the bottom of the snowpack were sometimes missing due to

unavoidable thawing and re-freezing near the ground (e.g., Fig. 3). When this occurred alongside turbulent conditions, diffusive flux uncertainty from the bottom of the snowpack was high, and this translated to high total flux uncertainty. Despite this occasional high flux uncertainty, our analysis detected significant shifts in wintertime soil respiration from year to year which could not have been detected from only EC fluxes.

Our study co-occurred with a bark beetle outbreak that began in 2008 and killed trees over the course of about 3 years. Such mortality events have unclear effects on soil respiration, with some studies showing no effect over the first few years (Morehouse et al., 2008; Borkhuu et al., 2015; Speckman et al., 2015; Barba et al., 2016) and yet others showing small and/or transient negative effects (Moore et al., 2013; Levy-Varon et al., 2014). In contrast to past field measurements, we found evidence for a short-lived pulse in wintertime respiration in 2011, 1-year following near-complete loss of needles from affected trees and 3 years after the onset of beetle infestation (Fig. 7). This pattern corresponded to critical stages of detrital production and understory recovery in the forest (Frank et al., 2014). Our finding is supported by ecosystem model predictions of a pulse in soil respiration following bark beetle attack fueled by detritus from the mortality event (Edburg et al., 2011).

However, a previous study at GLEES found no effect of mortality on soil respiration measured during the growing season (Speckman et al., 2015). We propose that mortality effects on soil respiration that are not pronounced during the growing season may be more detectable during the winter. First, trees are dormant during the winter, so heterotrophic soil respiration should dominate the respiration signal (although see Tucker et al. (2014)). Further, snowpack insulates the soil surface from below-freezing temperatures and buffers the soil against temperature and moisture fluctuations which otherwise create noise in growing season soil respiration (Lloyd and Taylor, 1994; Davidson et al., 1998; Wang et al., 2013). Underneath persistent winter snowpack, heterotrophic respiration is highly responsive to the amount of labile substrate available for respiration (Brooks et al., 2004). The timing of the 2011 pulse in respiration in our study is consistent with rapid heterotrophic consumption of a labile C substrate addition to the soil immediately after needle drop by affected trees in 2010.

In addition to the short-term increase in respiration following mortality, we detected a secondary rise in respiration during the last 3 years of the study. This rise follows an increase in leaf area index as understory trees and other vegetation boost their growth following overstory mortality. Increased growing season photosynthesis during this recovery may have resulted in increased winter soil respiration (Zhao et al., 2016). Another potential covariate is soil moisture under snowpack which may be an important influence on wintertime soil respiration (Mast et al., 1998; Contosta et al., 2016; Knowles et al., 2016), so it is possible that interannual changes in soil moisture may have confounded or contributed to the mortality effect. Parsing out individual drivers of variability in wintertime soil respiration from year to year will help advance our understanding of the C cycle in subalpine forests.

Our findings build on a body of work that collectively emphasizes the importance of winter C flux measurements in high-altitude/latitude systems with persistent snowpack (Liptzin et al., 2009; Björkman et al., 2010; Brooks et al., 2011). Measuring wintertime soil respiration at a similar time scale to that of EC fluxes allowed us to conclude that advection decoupled snowpack CO_2 efflux from biological production, a common occurrence in this forest ecosystem. Despite the presence of advection, past survey measurements were within the same range as our minitower wintertime soil respiration fluxes. Even though the minitowers sacrified high spatial resolution for added temporal resolution, the general agreement between EC and minitower methods suggests that three to four minitower replicates is mostly sufficient to characterize wintertime soil respiration at a similar spatial scale to EC. Thus, from an ecological standpoint, the main advantage of our high-frequency sampling and Bayesian approach is increased confidence in annual average wintertime soil respiration, which allowed a detection of a significant interannual trend even when accounting for measurement uncertainty due to missing values and strong advection. Assuming that wintertime soil respiration is unvaried from year to year and/or reliance only on EC for wintertime respiration could mislead efforts to close annual C budgets where snowpack persists for several months out of the year.

Acknowledgements

This work was funded by the U.S. Forest Service, the AmeriFlux program, and the Climate and Land Use Change Mission Area of U.S. Geological Survey. We acknowledge the assistance of Brianna Miles for collection of snowpack survey CO_2 measurements and Dr. Jace Fahnestock for the use of his data. We also thank Monica Dorning and anonymous peer reviewers, whose comments and suggestions improved the quality of this paper. Any use of trade, product or firm names is for descriptive purposes only and does not imply endorsement by the U.S. Government. All data and R code for analysis can be found at the USGS ScienceBase Catalog (Berryman et al., 2017).

Appendix A. Snowpack development model

The modeled total snowpack height ($\hat{h}_j$) for each day (j) is the sum of the modeled state variables corresponding to the height ($\hat{h}_{j,l}$) of each snowpack layer (l) (Eq. (15)). The convention is that once a layer l is established on day j (i.e., $l = j$ on that day), then it persists as a unique entity for the remainder of the winter.

$$\hat{h}_j = \sum_{l=1}^{j} \hat{h}_{j,l} \tag{15}$$

The height of each layer is associated with the mass of precipitation (P_l) that fell on day l, modified by the empirical coefficient a and divided by the state variable corresponding to the modeled snow density ($\hat{\rho}_{\text{snow},t,l}$) of each layer (Eq. (16)).

$$\hat{h}_{j,l} = a\frac{P_l}{\hat{\rho}_{\text{snow},j,l}} \tag{16}$$

The modeled snow density is a function of precipitation and time

$$\hat{\rho}_{\text{snow},j,l} = \frac{\{b_1 + b_2[1 - e^{-b_3(j-l)}]\}\left\{(1 - c_1) + c_1 e^{-\left[\frac{\left(\sum_{i=l}^{j} P_l\right) - c_2}{c_3}\right]^2}\right\}}{1 + e^{-d_1[(\sum_{i=1}^{l} P_l) - d_2]}} \tag{17}$$

where the first term (with coefficients b_{1-3}) is associated with settling of fresh snow based on the number of days since the layer was formed (i.e., $j - l$), the second term (with coefficients c_{1-3}) is a Gaussian function associated with snow compaction from the weight of snow above each layer, and the third term (with coefficients d_{1-2}) is associated with the formation of depth hoar near the soil surface which tends to decrease the density.

Simultaneously, the measured density profile, $\rho_{snow,z}$, is predicted for individual snow pits as a function of depth above the soil surface (z, m) with a Gaussian function with coefficients e_{1-3} (Eq. (18)).

$$\rho_{\mathrm{snow},z} = e_1 e^{-\left[\frac{z/h - e_2}{e_3}\right]^2} \tag{18}$$

The parameters of interest are a, b_{1-3}, c_{1-3}, and d_{1-2}, which are obtained by running a Bayesian analysis (Gelman et al., 2014) where all daily snowpack observations are predicted from a normal distribution with a mean defined by Eq. (15) and all snow pit density profile samples predicted from a gamma distribution with an expected value defined by Eq. (18). For both data sets, the standard deviation of the predictions are defined with prior gamma distributions. For all days with snow pit data, the Bayesian model applies Eq. (18) to fit the state variables $\hat{h}_{j,l}$ and $\hat{\rho}_{\mathrm{snow},j,l}$ using the same parameters e_{1-3} that are used to fit the snow pit data. In other words, Eqs. (16) and (17) are used to construct a "dummy" data set of depth and density profiles based only on P, and the Bayesian model uses Eq. (18) to fit to both the observed snow pit data and the "dummy" data. This leads to an optimal parameterization for a, b_{1-3}, c_{1-3}, and d_{1-2} to predict a snowpack with both realistic depth and density.

After the posterior distributions for the parameters a, b_{1-3}, c_{1-3}, and d_{1-2} are obtained, the Bayesian cut function (Plummer, 2015) is utilized to predict the snow height and density for each day from the winters 2009–2016. The Gaussian function (Eq. (18)) is then fit to each multilayer profile for each day (t) to obtain $e_{1,j}$, $e_{2,j}$, and $e_{3,j}$. The Bayesian cut function is important in this step because otherwise the act of fitting Eq. (18) to each day will create posterior distributions for parameters a, b_{1-3}, c_{1-3}, and d_{1-2} that are very different than the distributions obtained from the analysis of the snow accumulation model. The average daily snow density was then calculated as

$$\overline{\rho}_{\mathrm{snow},j} = \frac{\sqrt{\pi}\, e_{1,j} e_{3,j}}{2}\left[\mathrm{erf}\left(\frac{1 - e_{2,j}}{e_{3,j}}\right) - \mathrm{erf}\left(-\frac{e_{2,j}}{e_{3,j}}\right)\right] \tag{19}$$

The local variation of snowpack near each Replicate is quantified through interpolation with the continuous h measurement. Snow temperature is modeled at each Replicate from the heat equation, which is solved numerically using the explicit finite difference method. The upper boundary condition for snow temperature is assumed to be the black body temperature associated with upwelling longwave radiation measured at US-GLE and the lower boundary and initial conditions are assumed to be 0 °C. The parameters $e_{1,j}$, $e_{2,j}$, and $e_{3,j}$ are used to evaluate Gaussian snow density profiles for each day from Eq. (18) which are then interpolated into half-hourly values. Thermal conductivity of snow is predicted from its density (Sturm et al., 1997). The heat equation is solved by dividing the snowpack from top to bottom into 5.5 cm thick layers and solving for every half-hour. The resulting temperature profile is averaged and resampled to once an hour.

Appendix B. CO_2 profile-based model for inferring diffusive & advective fluxes

Estimating diffusive fluxes requires differentiating Eq. (1), which yields the following expression for the model gradient of the CO_2 profile as a function of depth:

$$\frac{\partial \chi_c}{\partial z} = -\frac{\chi_B}{h}\left[\frac{2\alpha}{\sqrt{\pi}}\right]\left[\frac{\exp(-\alpha^2 z^2/h^2)}{\mathrm{erf}(\alpha)}\right] \tag{20}$$

which in turn further yields the gradient at the top of the snowpack:

$$\frac{\partial \chi_c}{\partial z}(1) = -\frac{\chi_B}{h}\left[\frac{2\alpha}{\sqrt{\pi}}\right]\left[\frac{\exp(-\alpha^2)}{\mathrm{erf}(\alpha)}\right] \tag{21}$$

and the gradient at the bottom of the snowpack:

$$\frac{\partial \chi_c}{\partial z}(0) = -\frac{\chi_B}{h}\left[\frac{2\alpha}{\sqrt{\pi}\,\mathrm{erf}(\alpha)}\right] \tag{22}$$

These terms are then combined with snowpack properties in Eq. (2) to calculate $J_{diff}(0)$ and $J_{diff}(1)$.

Eq. (3) is then evaluated for S_{0h}.

$$S_{0h} = \overline{\rho_{\mathrm{da}}} \int_0^h \frac{\partial \chi_c}{\partial t}\,\mathrm{d}z \equiv \overline{\rho_{\mathrm{da}}}\ \mathscr{I}_\chi \tag{23}$$

$\mathscr{I}_\chi$ is introduced here to help simplify the mathematical development of S_{0h} as follows.

$\chi_c(0)$, χ_B, and α are functions of time, i.e., $\chi_c(0) = \chi_c(0, t)$, $\chi_B = \chi_B(t)$, and $\alpha = \alpha(t)$. Snowpack height h can vary in time; although, unless snowing vigorously, h is not expected to vary from one hour to the next as much as the three fitting parameters might. Employing Leibnitz's rule to move the time derivative outside the integral it follows that

$$\mathscr{I}_\chi \equiv \int_0^h \frac{\partial \chi_c}{\partial t}\mathrm{d}z = \frac{\partial}{\partial t}\int_0^h \chi_c\,\mathrm{d}z - \chi_c(1)\frac{\partial h}{\partial t} = h\frac{\partial \chi_c(1)}{\partial t} + \frac{\partial}{\partial t}\left[\frac{h^2}{2\alpha^2}\Delta_c(1)\right] \tag{24}$$

where

$$\int_0^h \chi_c\,\mathrm{d}z = h\,\chi_c(1) + \frac{h^2}{2\alpha^2}\Delta_c(1) \tag{25}$$

and

$$\Delta_c(1) \equiv \frac{\partial \chi_c}{\partial z}(0) - \frac{\partial \chi_c}{\partial z}(1) = -\frac{\chi_B}{h}\left[\frac{2\alpha}{\sqrt{\pi}}\right]\left[\frac{1-\exp(-\alpha^2)}{\mathrm{erf}(\alpha)}\right] \tag{26}$$

Expanding the right-most term of Eq. (24) yields:

$$\frac{\partial}{\partial t}\left[\frac{h^2}{2\alpha^2}\Delta_c(1)\right] = h\frac{\partial \chi_c(1)}{\partial t} + \left(\frac{h}{\alpha^2}\Delta_c(1)\right)\frac{\partial h}{\partial t} - \left(\frac{h^2}{\alpha^3}\Delta_c(1)\right)\frac{\partial \alpha}{\partial t} + \tag{27}$$

$$\left(\frac{h^2}{2\alpha^2}\right)\frac{\partial \Delta_c(1)}{\partial t} \tag{28}$$

By the chain rule

$$\frac{\partial \Delta_c(1)}{\partial t} = \frac{\partial h}{\partial t}\frac{\partial \Delta_c(1)}{\partial h} + \frac{\partial \alpha}{\partial t}\frac{\partial \Delta_c(1)}{\partial \alpha} + \frac{\partial \chi_B}{\partial t}\frac{\partial \Delta_c(1)}{\partial \chi_B} \tag{29}$$

and by differentiation of Eq. (26)

$$\frac{\partial \Delta_c(1)}{\partial h} = -\frac{\Delta_c(1)}{h} \tag{30}$$

$$\frac{\partial \Delta_c(1)}{\partial \alpha} = \left[\frac{1}{\alpha} - \frac{2\exp(-\alpha^2)}{\sqrt{\pi}\,\mathrm{erf}(\alpha)}\right]\Delta_c(1) + 2\alpha\frac{\partial \chi_c}{\partial z}(1) \tag{31}$$

and

$$\frac{\partial \Delta_c(1)}{\partial \chi_B} = -\frac{1}{h}\left[\frac{2\alpha}{\sqrt{\pi}}\right]\left[\frac{1-\exp(-\alpha^2)}{\mathrm{erf}(\alpha)}\right] = \frac{\Delta_c(1)}{\chi_B} \tag{32}$$

With these last three partial derivatives of $\Delta_c(1)$ and after some simplification the final expression for $\mathscr{I}_\chi$ is

$$\mathscr{I}_\chi = h\frac{\partial \chi_c(1)}{\partial t} + \left(\frac{h}{2\alpha^2}\Delta_c(1)\right)\frac{\partial h}{\partial t} + \left(\frac{h^2}{2\alpha^2}\frac{\partial \Delta_c(1)}{\partial \chi_B}\right)\frac{\partial \chi_B}{\partial t} + \frac{h^2}{\alpha^2}\left(-\frac{\Delta_c(1)}{\alpha} + \frac{1}{2}\frac{\partial \Delta_c(1)}{\partial \alpha}\right)\frac{\partial \alpha}{\partial t} \tag{33}$$

Evaluating $\mathscr{I}_\chi$ for every hour of observed profile data requires that the four time derivatives $\partial\chi_c(1)/\partial t$, $\partial\chi_B/\partial t$, $\partial\alpha/\partial t$, and $\partial h/\partial t$ be determined numerically, which is accomplished with a standard second order center-difference scheme operating on the four (temporally discrete) time series $\chi_c(0, t)$, $\chi_B(t)$, $\alpha(t)$, and $h(t)$. With this the model of the storage term is complete.

The rationale behind Eq. (5) relating $J_{adv}(0)$ to $J_{adv}(1)$ is as follows. α is included because we hypothesize that stronger advective forcing (increasing α) will penetrate deeper through the snowpack and into the soil and thereby force a proportional increase in $J_{adv}(0)$. But there remains a lot of freedom (uncertainty) for choosing a numerical value for β. Eq. (5) can be interpreted in terms of a linear forcing and response type of model, for which β would be a transfer function and could then be parameterized as a function of the properties of the snowpack (e.g., permeability, dispersivity, porosity). Massman (2006) developed a model of pressure pumping of snowpacks along similar lines. But he did not seek a quantitative relationship between the advective fluxes. Nevertheless, his results suggest that $J_{adv}(1) > J_{adv}(0)$, which implies that $\beta\alpha < 1$ can be reasonably assumed. This is consistent with the expectation that the advective forcing is always stronger at the top of the snowpack than at the bottom. (Note: It is conceivable that the opposite is true, i.e., $J_{adv}(1) \leq J_{adv}(0) \neq 0$; but no CO_2 snowpack profile observed in this study comes close to approximating the snowpack CO_2 profile associated with this condition.) Combining the constraint that $\beta\alpha < 1$ with the observation that $\alpha < 5$ for all profiles in the present GLEES data, we can further conclude that $\beta \leq 0.2$ can be expected. Therefore, in keeping with the desire for simplicity we assume that $\beta = 0.02$, a constant with a range of uncertainty between 0.002 and 0.2 (which spans two orders of magnitude), and we admit quite freely that this value for β is heuristic and, at some level even, arbitrary.

References

Barba, J., Yuste, J.C., Poyatos, R., Janssens, I.A., Lloret, F., 2016. Strong resilience of soil respiration components to drought-induced die-off resulting in forest secondary succession? Oecologia 182 (1), 27–41.

Berryman, E., Ryan, M.G., Bradford, J.B., Hawbaker, T.J., Birdsey, R., 2016. Total belowground carbon flux in subalpine forests is related to leaf area index, soil nitrogen, and tree height. Ecosphere 7 (8).

Berryman, E.M., Frank, J.M., Massman, W.J., Ryan, M.G., Fahnestock, J., 2017. Advective and Diffusive Snowpack Carbon Dioxide Fluxes from 2009 to 2016 at GLEES. U.S. Geological Survey Data Release, Wyoming. http://dx.doi.org/10.5066/F7K35SJH.

Björkman, M.P., Morgner, E., Cooper, E.J., Elberling, B., Klemedtsson, L., Björk, R.G., 2010. Winter carbon dioxide effluxes from Arctic ecosystems: an overview and comparison of methodologies. Global Biogeochem. Cycles 24 (3), GB3010.

Borkhuu, B., Peckham, S.D., Ewers, B.E., Norton, U., Pendall, E., 2015. Does soil respiration decline following bark beetle induced forest mortality? Evidence from a lodgepole pine forest. Agric. For. Meteorol. 214–215, 201–207.

Bowling, D.R., Massman, W.J., 2011. Persistent wind-induced enhancement of diffusive CO_2 transport in a mountain forest snowpack. J. Geophys. Res. 116, G04006.

Brooks, P.D., Grogan, P., Templer, P.H., Groffman, P., Öquist, M.G., Schimel, J., 2011. Carbon and nitrogen cycling in snow-covered environments? Geogr. Compass 5 (9), 682–699.

Brooks, P.D., McKnight, D., Elder, K., 2004. Carbon limitation of soil respiration under winter snowpacks: potential feedbacks between growing season and winter carbon fluxes. Glob. Change Biol. 11, 231–238.

Burba, G., McDermitt, D., Grelle, A., Anderson, D., Xu, L., 2008. Addressing the influence of instrument surface heat exchange on the measurements of CO_2 flux from open-path gas analyzers? Glob. Change Biol. 14 (8), 1854–1876.

Carbone, M.S., Vargas, R., 2008. Automated soil respiration measurements: new information, opportunities, and challenges. New Phytol. 177, 295–297.

Contosta, A.R., Burakowski, E.A., Varner, R.K., Frey, S.D., 2016. Winter soil respiration in a humid temperate forest: the roles of moisture, temperature, and snowpack. J. Geophys. Res. Biogeosci 2016JG003450.

Davidson, E.A., Belk, E., Boone, R.D., 1998. Soil water content and temperature as independent or confounded factors controlling soil respiration in a temperate mixed hardwood forest. Glob. Change Biol. 4, 217–227.

Edburg, S.L., Hicke, J.A., Lawrence, D.M., Thornton, P.E., 2011. Simulating coupled carbon and nitrogen dynamics following mountain pine beetle outbreaks in the western United States. J. Geophys. Res. 116, G04033.

Euskirchen, E.S., Bret-Harte, M.S., Scott, G.J., Edgar, C., Shaver, G.R., 2012. Seasonal patterns of carbon dioxide and water fluxes in three representative tundra ecosystems in northern Alaska? Ecosphere 3 (1), 1–19.

Frank, J.M., Massman, W.J., Ewers, B.E., 2013. Underestimates of sensible heat flux due to vertical velocity measurement errors in non-orthogonal sonic anemometers. Agric. For. Meteorol. 171, 72–81.

Frank, J.M., Massman, W.J., Ewers, B.E., Huckaby, L.S., Negrón, J.F., 2014. Ecosystem CO_2/H_2O fluxes are explained by hydraulically limited gas exchange during tree

mortality from spruce bark beetles. J. Geophys. Res. Biogeosci. 119, 1195–1215.
Gelman, A., Carlin, J.B., Stern, H.S., Dunson, D.B., Vehtari, A., Rubin, D.B., 2014. Bayesian Data Analysis, 3rd ed. CRC Press, Boca Raton, FL.
Hubbard, R.M., Ryan, M.G., Elder, K., Rhoades, C.C., 2005. Seasonal patterns in soil surface CO_2 flux under snow cover in 50 and 300 year old subalpine forests. Biogeochemistry 73, 93–107.
Knowles, J.F., Blanken, P.D., Williams, M.W., 2016. Wet meadow ecosystems contribute the majority of over-winter soil respiration from snow-scoured alpine tundra. J. Geophys. Res. Biogeosci 2015JG003081.
Kruschke, J., 2014. Doing Bayesian Data Analysis: A Tutorial with R, JAGS, and Stan. Academic Press.
Kruschke, J.K., 2013. Bayesian estimation supersedes the *t* test. J. Exp. Psychol.: Gen. 142 (2), 573.
Levy-Varon, J.H., Schuster, W.S.F., Griffin, K.L., 2014. Rapid rebound of soil respiration following partial stand disturbance by tree girdling in a temperate deciduous forest. Oecologia 174, 1415–1424.
Liptzin, D., Williams, M., Helmig, D., Seok, B., Filippa, G., Chowanski, K., Hueber, J., 2009. Process-level controls on CO_2 fluxes from a seasonally snow-covered subalpine meadow soil, Niwot Ridge, Colorado. Biogeochemistry 95, 151–166.
Lloyd, J., Taylor, J.A., 1994. On the temperature dependence of soil respiration. Funct. Ecol. 8, 315–323.
Massman, W.J., 2006. Advective transport of CO2 in permeable media induced by atmospheric pressure fluctuations: 1. An analytical model. J. Geophys. Res. 111, G003004.
Massman, W., Sommerfeld, R., Zeller, K., Hehn, T., Hudnell, L., Rochelle, S., 1995. CO_2 flux through a Wyoming seasonal snowpack: diffusional and pressure pumping effects. Biogeochemistry of Seasonally Snow-Covered Catchments (Proceedings of a Boulder Symposium, July 1995).
Massman, W.J., Sommerfeld, R.A., Mosier, A.R., Zeller, K.F., Hehn, T.J., Rochelle, S.G., 1997. A model investigation of turbulence-driven pressure-pumping effects on the rate of diffusion of CO_2, N_2O, and CH_4 through layered snowpacks. J. Geophys. Res. 102 (D15), 18851–18863.
Mast, M.A., Wickland, K.P., Striegl, R.T., Clow, D.W., 1998. Winter fluxes of CO_2 and CH_4 from subalpine soils in Rocky Mountain National Park, Colorado. Global Biogeochem. Cycles 12, 607–620.
McDowell, N.G., Marshall, J.D., Hooker, T.D., Musselman, R., 2000. Estimating CO_2 flux from snowpacks at three sites in the Rocky Mountains. Tree Physiol. 20, 745–753.
McGuire, A.D., Melillo, J.M., Randerson, J.T., Parton, W.J., Heimann, M., Meier, R.A., Clein, J.S., Kicklighter, D.W., Sauf, W., 2000. Modeling the effects of snowpack on heterotrophic respiration across northern temperate and high latitude regions: comparison with measurements of atmospheric carbon dioxide in high latitudes. Biogeochemistry 48, 91–114.
Moore, D.J.P., Trahan, N.A., Wilkes, P., Quaife, T., Stephens, B.B., Elder, K., Desai, A.R., Negron, J., Monson, R.K., 2013. Persistent reduced ecosystem respiration after insect disturbance in high elevation forests. Ecol. Lett. 16, 731–737.
Morehouse, K., Johns, T., Kaye, J., Kaye, M., 2008. Carbon and nitrogen cycling immediately following bark beetle outbreaks in southwestern ponderosa pine forests. For. Ecol. Manag. 255, 2698–2708.
Musselman, R.C., Massman, W.J., Frank, J.M., Korfmacher, J.L., 2005. The temporal dynamics of carbon dioxide under snow in a high elevation Rocky Mountain subalpine forest and meadow. Arct. Antarct. Alp. Res. 37, 527–538.
Phillips, C.L., Bond-Lamberty, B., Desai, A.R., Lavoie, M., Risk, D., Tang, J., Todd-Brown, K., Vargas, R., 2016. The value of soil respiration measurements for interpreting and modeling terrestrial carbon cycling. Plant Soil 1–25.
Plummer, M., 2003. JAGS: a program for analysis of Bayesian graphical models using Gibbs sampling. In: Proceedings of the 3rd International Workshop on Distributed Statistical Computing (DSC 2003), vol. 124. March 20–22, Vienna, Austria. Technische Universit at Wien.
Plummer, M., 2011. Generating Data From A Stochastic Model… JAGS: Just Another Gibbs Sampler. https://sourceforge.net/p/mcmc-jags/discussion/610037/thread/71466030/.
Plummer, M., 2015. Cuts in Bayesian graphical models? Stat. Comput. 25 (1), 37–43.
Plummer, M., 2017. rjags: Bayesian graphical models using MCMC, version 4-4. R package. http://CRAN.R-project.org/package=rjags.
Plummer, M., Best, N., Cowles, K., Vines, K., 2006. CODA: Convergence Diagnosis and Output Analysis for MCMC. RNEWS Vol. 61 R Foundation, Vienna, Austria. https://www.r-project.org/doc/Rnews/Rnews_2006-1.pdf.
Core Team, R., 2016. R: A Language and Environment for Statistical Computing. R Foundation for Statistical Computing, Vienna, Austria.
Ryan, M.G., Law, B.E., 2005. Interpreting, measuring and modeling soil respiration. Biogeochemistry 73, 3–27.
Schöpf, H., Supancic, P., 2014. On Bürmann's Theorem and its application to problems of linear and nonlinear heat transfer and diffusion. Math. J. 6, 1–44.
Seok, B., Helmig, D., Williams, M.W., Liptzin, D., Chowanski, K., Hueber, J., 2009. An automated system for continuous measurements of trace gas fluxes through snow: an evaluation of the gas diffusion method at a subalpine forest site, Niwot Ridge, Colorado. Biogeochemistry 95 (1), 95–113.
Sommerfeld, R., Musselman, R., Reuss, J., Mosier, A., 1991. Preliminary measurements of CO_2 in melting snow? Geophys. Res. Lett. 18 (7), 1225–1228.
Sommerfeld, R.A., Massman, W.J., Musselman, R.C., 1996. Diffusional flux of CO_2 through snow: spatial and temporal variability among alpine-subalpine sites. Global Biogeochem. Cycles 10, 473–482.
Sommerfeld, R.A., Mosier, A.R., Musselman, R.C., 1993. CO_2, CH_4, and N_2O flux through a Wyoming snowpack and implications for global budgets. Nature 361, 140–142.
Speckman, H.N., Frank, J.M., Bradford, J.B., Miles, B.L., Massman, W.J., Parton, W.J., Ryan, M.G., 2015. Forest ecosystem respiration estimated from eddy covariance and chamber measurements under high turbulence and substantial tree mortality from bark beetles. Glob. Change Biol. 21, 708–721.
Spiegelhalter, D.J., Best, N.G., Carlin, B.P., Van Der Linde, A., 2002. Bayesian measures of model complexity and fit? J. R. Stat. Soc.: Ser. B (Stat. Methodol.) 64 (4), 583–639.
Spiegelhalter, D.J., Best, N.G., Carlin, B.P., van der Linde, A., 2014. The deviance information criterion: 12 years on? J. R. Stat. Soc.: Ser. B (Stat. Methodol.) 76 (3), 485–493.
Sturm, M., Holmgren, J., König, M., Morris, K., 1997. The thermal conductivity of seasonal snow? J. Glaciol. 43 (143), 26–41.
Takagi, K., Nomura, M., Ashiya, D., Takahashi, H., Sasa, K., Fujinuma, Y., Shibata, H., Akibayashi, Y., Koike, T., 2005. Dynamic carbon dioxide exchange through snowpack by wind-driven mass transfer in a conifer-broadleaf mixed forest in northernmost Japan. Global Biogeochem. Cycles 19, GB2012.
Tucker, C.L., Tamang, S., Pendall, E., Ogle, K., 2016. Shallow snowpack inhibits soil respiration in sagebrush steppe through multiple biotic and abiotic mechanisms. Ecosphere 7 (5).
Tucker, C.L., Young, J.M., Williams, D.G., Ogle, K., 2014. Process-based isotope partitioning of winter soil respiration in a subalpine ecosystem reveals importance of rhizospheric respiration. Biogeochemistry 1–20.
van Asperen, H., Warneke, T., Sabbatini, S., Höpker, M., Nicolini, G., Chiti, T., Papale, D., Böhm, M., Notholt, J., 2017. Diel variation in isotopic composition of soil respiratory CO_2 fluxes: the role of non-steady state conditions. Agric. For. Meteorol. 234-235, 95–105.
Vargas, R., Allen, M.F., 2008. Environmental controls and the influence of vegetation type, fine roots and rhizomorphs on diel and seasonal variation in soil respiration. New Phytol. 460–471.
Wang, C., Han, Y., Chen, J., Wang, X., Zhang, Q., Bond-Lamberty, B., 2013. Seasonality of soil CO_2 efflux in a temperate forest: biophysical effects of snowpack and spring freeze-thaw cycles. Agric. For. Meteorol. 177, 83–92.
Webb, E.E., Schuur, E.A.G., Natali, S.M., Oken, K.L., Bracho, R., Krapek, J.P., Risk, D., Nickerson, N.R., 2016. Increased wintertime CO_2 loss as a result of sustained tundra warming. J. Geophys. Res. Biogeosci. 121 (2) 2014JG002795.
Zhao, J., Peichl, M., Öquist, M., Nilsson, M.B., 2016. Gross primary production controls the subsequent winter CO_2 exchange in a boreal peatland? Glob. Change Biol. 22 (12), 4028–4037.